Search for pair production of neutral Higgs bosons in Z^0 decays

DELPHI Collaboration

P. Abreu [a], W. Adam [b], F. Adami [c], T. Adye [d], G.D. Alekseev [e], J.V. Allaby [f], P. Allen [g], S. Almehed [h], F. Alted [g], S.J. Alvsvaag [i], U. Amaldi [f], E. Anassontzis [j], W.D. Apel [k], B. Asman [l], C. Astor Ferreres [m], J.E. Augustin [n], A. Augustinus [f], P. Baillon [f], P. Bambade [n], F. Barao [a], G. Barbiellini [o], D.Yu. Bardin [e], A. Baroncelli [p], O. Barring [h], W. Bartl [b], M.J. Bates [q], M. Baubillier [r], K.H. Becks [s], C.J. Beeston [q], P. Beilliere [t], I. Belokopytov [u], P. Beltran [v], D. Benedic [w], J.M. Benlloch [g], M. Berggren [l], D. Bertrand [x], S. Biagi [y], F. Bianchi [z], J.H. Bibby [q], M.S. Bilenky [e], P. Billoir [r], J. Bjarne [h], D. Bloch [w], P.N. Bogolubov [e], D. Bollini [α], T. Bolognese [c], M. Bonapart [β], P.S.L. Booth [y], M. Boratav [r], P. Borgeaud [c], H. Borner [q], C. Bosio [p], O. Botner [γ], B. Bouquet [n], M. Bozzo [δ], S. Braibant [f], P. Branchini [p], K.D. Brand [s], R.A. Brenner [ε], C. Bricman [x], R.C.A. Brown [f], N. Brummer [β], J.M. Brunet [t], L. Bugge [ζ], T. Buran [ζ], H. Burmeister [f], C.M. Buttar [q], J.A.M.A. Buytaert [x], M. Caccia [η], M. Calvi [η], A.J. Camacho Rozas [m], J.E. Campagne [f], A. Campion [y], T. Camporesi [f], V. Canale [p], F. Cao [x], L. Carroll [y], C. Caso [δ], E. Castelli [o], M.V. Castillo Gimenez [g], A. Cattai [f], F.R. Cavallo [α], L. Cerrito [p], P. Charpentier [f], P. Checchia [θ], G.A. Chelkov [e], L. Chevalier [c], P.V. Chliapnikov [u], V. Chorowicz [r], R. Cirio [z], M.P. Clara [z], J.L. Contreras [g], R. Contri [δ], G. Cosme [n], F. Couchot [n], H.B. Crawley [κ], D. Crennell [d], M. Cresti [θ], G. Crosetti [δ], N. Crosland [q], M. Crozon [t], J. Cuevas Maestro [m], S. Czellar [ε], S. Dagoret [n], E. Dahl-Jensen [λ], B. D'Almagne [n], M. Dam [f], G. Damgaard [λ], G. Darbo [δ], E. Daubie [x], M. Davenport [f], P. David [r], A. De Angelis [o], M. De Beer [c], H. De Boeck [x], W. De Boer [k], C. De Clercq [x], M.D.M. De Fez Laso [g], N. De Groot [β], C. De La Vaissiere [r], B. De Lotto [o], C. Defoix [t], D. Delikaris [f], P. Delpierre [t], N. Demaria [z], A. De Min [η], L. Di Ciaccio [p], A.N. Diddens [β], H. Dijkstra [f], F. Djama [w], J. Dolbeau [t], K. Doroba [μ], M. Dracos [w], J. Drees [s], M. Dris [ξ], W. Dulinski [w], R. Dzhelyadin [u], D.N. Edwards [y], L.O. Eek [γ], P.A.M. Eerola [ε], T. Ekelof [γ], G. Ekspong [l], J.P. Engel [w], V. Falaleev [u], A. Fenyuk [u], M. Fernandez Alonso [m], A. Ferrer [g], S. Ferroni [δ], T.A. Filippas [ξ], A. Firestone [κ], H. Foeth [f], E. Fokitis [ξ], F. Fontanelli [δ], H. Forsbach [s], B. Franek [d], K.E. Fransson [γ], P. Frenkiel [t], D.C. Fries [k], R. Fruhwirth [b], F. Fulda-Quenzer [n], H. Fuerstenau [k], J. Fuster [f], J.M. Gago [a], G. Galeazzi [θ], D. Gamba [z], U. Gasparini [θ], P. Gavillet [f], S. Gawne [y], E.N. Gazis [ξ], P. Giacomelli [α], K.W. Glitza [s], R. Gokieli [r], V.M. Golovatyuk [e], A. Goobar [l], G. Gopal [d], M. Gorski [μ], V. Gracco [δ], A. Grant [f], F. Grard [x], E. Graziani [p], M.H. Gros [n], G. Grosdidier [n], B. Grossetete [r], S. Gumenyuk [u], J. Guy [d], F. Hahn [s], M. Hahn [k], S. Haider [f], Z. Hajduk [π], A. Hakansson [h], A. Hallgren [γ], K. Hamacher [s], G. Hamel De Monchenault [c], J.F. Harris [q], B. Heck [f], I. Herbst [s], J.J. Hernandez [g], P. Herquet [x], H. Herr [f], E. Higon [g], H.J. Hilke [f], T. Hofmokl [μ], R. Holmes [κ], S.O. Holmgren [l], J.E. Hooper [λ], M. Houlden [y], J. Hrubec [b], P.O. Hulth [l], K. Hultqvist [l], D. Husson [w], B.D. Hyams [f], P. Ioannou [j], P.S. Iversen [i], J.N. Jackson [y], P. Jalocha [π], G. Jarlskog [h], P. Jarry [c], B. Jean-Marie [n], E.K. Johansson [l], M. Jonker [f], L. Jonsson [h], P. Juillot [w], R.B. Kadyrov [e], G. Kalkanis [j], G. Kalmus [d], G. Kantardjian [f], F. Kapusta [r], P. Kapusta [π], S. Katsanevas [j], E.C. Katsoufis [ξ], R. Keranen [ε], J. Kesteman [x], B.A. Khomenko [e], B. King [y], N.J. Kjaer [λ], H. Klein [f], W. Klempt [f], A. Klovning [i], P. Kluit [x], J.H. Koehne [k], B. Koene [β], P. Kokkinias [v],

0370-2693/90/$ 03.50

M. Kopf [k], M. Koratzinos [f], K. Korcyl [π], A.V. Korytov [e], B. Korzen [f], C. Kourkoumelis [j], T. Kreuzberger [b], J. Krolikowski [μ], U. Kruener-Marquis [s], W. Krupinski [π], W. Kucewicz [η], K. Kurvinen [ε], M.I. Laakso [ε], C. Lambropoulos [ν], J.W. Lamsa [κ], L. Lanceri [o], V. Lapin [u], J.P. Laugier [c], R. Lauhakangas [ε], P. Laurikainen [ε], G. Leder [b], F. Ledroit [t], J. Lemonne [x], G. Lenzen [s], V. Lepeltier [n], A. Letessier-Selvon [r], E. Lieb [s], E. Lillestol [f], E. Lillethun [i], J. Lindgren [ε], I. Lippi [θ], R. Llosa [g], B. Loerstad [h], M. Lokajicek [e], J.G. Loken [q], A. Lopez [n], M.A. Lopez Aguera [m], D. Loukas [ν], J.J. Lozano [g], R. Lucock [d], B. Lund-Jensen [γ], P. Lutz [t], L. Lyons [q], G. Maehlum [f], J. Maillard [t], A. Maltezos [ν], F. Mandl [b], J. Marco [m], J.C. Marin [f], A. Markou [ν], L. Mathis [t], C. Matteuzzi [η], G. Matthiae [p], M. Mazzucato [θ], M. Mc Cubbin [y], R. Mc Kay [κ], E. Menichetti [z], C. Meroni [η], W.T. Meyer [κ], W.A. Mitaroff [b], G.V. Mitselmakher [e], U. Mjoernmark [h], T. Moa [ϱ], R. Moeller [λ], K. Moenig [s], M.R. Monge [δ], P. Morettini [δ], H. Mueller [k], H. Muller [f], G. Myatt [q], F. Naraghi [r], U. Nau-Korzen [s], F.L. Navarria [α], P. Negri [η], B.S. Nielsen [λ], M. Nigro [θ], V. Nikolaenko [u], V. Obraztsov [u], R. Orava [ε], A. Ouraou [c], R. Pain [r], K. Pakonski [π], H. Palka [π], T. Papadopoulou [ξ], L. Pape [f], P. Pasini [α], A. Passeri [p], M. Pegoraro [θ], V. Perevozchikov [u], M. Pernicka [b], M. Pimenta [a], O. Pingot [x], C. Pinori [θ], A. Pinsent [q], M.E. Pol [a], B. Poliakov [u], G. Polok [π], P. Poropat [o], P. Privitera [α], A. Pullia [η], J. Pyyhtia [ε], A.A. Rademakers [β], D. Radojicic [q], S. Ragazzi [η], W.H. Range [y], P.N. Ratoff [q], A.L. Read [ζ], N.G. Redaelli [η], M. Regler [b], D. Reid [y], P.B. Renton [q], L.K. Resvanis [j], F. Richard [n], J. Ridky [e], G. Rinaudo [z], I. Roditi [f], A. Romero [z], P. Ronchese [θ], E. Rosenberg [κ], U. Rossi [α], E. Rosso [f], P. Roudeau [n], T. Rovelli [α], V. Ruhlmann [c], A. Ruiz [m], H. Saarikko [ε], Y. Sacquin [c], E. Sanchez [g], J. Sanchez [g], E. Sanchis [g], M. Sannino [δ], M. Schaeffer [w], H. Schneider [k], F. Scuri [o], A. Sebastia [g], A.M. Segar [q], R. Sekulin [d], M. Sessa [o], G. Sette [δ], R. Seufert [k], R.C. Shellard [f], P. Siegrist [c], S. Simonetti [δ], F. Simonetto [θ], A.N. Sissakian [e], T.B. Skaali [ζ], J. Skeens [κ], G. Skjevling [ζ], G. Smadja [c], G.R. Smith [d], R. Sosnowski [μ], K. Spang [λ], T. Spassoff [e], E. Spiriti [p], S. Squarcia [δ], H. Staeck [s], C. Stanescu [p], G. Stavropoulos [ν], F. Stichelbaut [x], A. Stocchi [η], J. Strauss [b], R. Strub [w], C. Stubenrauch [f], M. Szczekowski [μ], M. Szeptycka [μ], P. Szymanski [μ], S. Tavernier [x], E. Tchernyaev [u], G. Theodosiou [ν], A. Tilquin [t], J. Timmermans [β], V.G. Timofeev [e], L.G. Tkatchev [e], D.Z. Toet [β], A.K. Topphol [i], L. Tortora [p], D. Treille [f], U. Trevisan [δ], G. Tristram [t], C. Troncon [η], E.N. Tsyganov [e], M. Turala [π], R. Turchetta [w], M.L. Turluer [c], T. Tuuva [ε], I.A. Tyapkin [e], M. Tyndel [d], S. Tzamarias [f], F. Udo [β], S. Ueberschaer [s], V.A. Uvarov [u], G. Valenti [α], E. Vallazza [z], J.A. Valls [g], G.W. Van Apeldoorn [β], P. Van Dam [β], W.K. Van Doninck [x], N. Van Eijndhoven [f], C. Vander Velde [x], J. Varela [a], P. Vaz [a], G. Vegni [η], M.E. Veitch [q], J. Velasco [g], L. Ventura [θ], W. Venus [d], F. Verbeure [x], L.S. Vertogradov [e], L. Vibert [r], D. Vilanova [c], N.K. Vishnevskiy [u], E.V. Vlasov [u], A.S. Vodopianov [e], M. Vollmer [s], G. Voulgaris [j], M. Voutilainen [ε], V. Vrba [e], H. Wahlen [s], C. Walck [ϱ], F. Waldner [o], M. Wayne [κ], P. Weilhammer [f], J. Werner [s], A.M. Wetherell [f], J.H. Wickens [x], J. Wikne [ζ], W.S.C. Williams [q], M. Winter [w], D. Wormald [ζ], G. Wormser [n], K. Woschnagg [γ], N. Yamdagni [ϱ], P. Yepes [β], A. Zaitsev [u], A. Zalewska [π], P. Zalewski [μ], P.I. Zarubin [e], E. Zevgolatakos [ν], G. Zhang [s], N.I. Zimin [e], R. Zitoun [r], R. Zukanovich Funchal [t], G. Zumerle [θ], J. Zuniga [g]

[a] *LIP, Av. Elias Garcia 14 - 1e, P-1000 Lisbon Codex, Portugal*
[b] *Institut für Hochenergiephysik, Österreichische Akademie der Wissenschaften, Nikolsdorfergasse 18, A-1050 Vienna, Austria*
[c] *DPhPE, CEN-Saclay, F-91191 Gif-Sur-Yvette Cedex, France*
[e] *Joint Institute for Nuclear Research, Dubna, Head Post Office, P.O. Box 79, SU-101 000 Moscow, USSR*
[f] *CERN, CH-1211 Geneva 23, Switzerland*
[g] *Instituto de Fisica Corpuscular (IFIC), Centro Mixto Universidad de Valencia–CSIC, Avda. Dr. Moliner 50, E-46100 Burjassot (Valencia), Spain*

[h] Department of Physics, University of Lund, Sölvegatan 14, S-223 63 Lund, Sweden
[i] Department of Physics, University of Bergen, Allégaten 55, N-5007 Bergen, Norway
[j] Physics Laboratory, University of Athens, Solonos Street 104, GR-10680 Athens, Greece
[k] Institut für Experimentelle Kernphysik, Universität Karlsruhe, Postfach 6980, D-7500 Karlsruhe 1, FRG
[l] Institute of Physics, University of Stockholm, Vanadisvägen 9, S-113 46 Stockholm, Sweden
[m] Facultad de Ciencias, Universidad de Santander, av. de los Castros, E-39005 Santander, Spain
[n] Laboratoire de l'Accélérateur Linéaire, Université de Paris-Sud, Bâtiment 200, F-91405 Orsay, France
[o] Dipartimento di Fisica, Università di Trieste and INFN, Via A. Valerio 2, I-34127 Trieste, Italy
and Istituto di Fisica, Università di Udine, Via Larga 36, I-33100 Udine, Italy
[p] Istituto Superiore di Sanità, Istituto Nazionale di Fisica Nucleare (INFN), Viale Regina Elena 299, I-00161 Rome, Italy
and Dipartimento di Fisica, Università di Roma II and INFN, Tor Vergata, I-00173 Rome, Italy
[q] Nuclear Physics Laboratory, University of Oxford, Keble Road, Oxford OX1 3RH, UK
[r] LPNHE, Universités Paris VI et VII, Tour 33 (RdC), 4 place Jussieu, F-75230 Paris Cedex 05, France
[s] Fachbereich Physik, University of Wuppertal, Postfach 100 127, D-5600 Wuppertal 1, FRG
[t] Laboratoire de Physique Corpusculaire, Collège de France, 11 place M. Berthelot, F-75231 Paris Cedex 5, France
[u] Institute for High Energy Physics, Serpukhov, P.O. Box 35, SU-142 284 Protvino (Moscow Region), USSR
[v] Greek Atomic Energy Commission, Nuclear Research Centre Demokritos, P.O. Box 60228, GR-15310 Aghia Paraskevi, Greece
[w] Division des Hautes Energies, CRN–Groupe DELPHI, B.P. 20 CRO, F-67037 Strasbourg Cedex, France
[x] Physics Department, Universitaire Instelling Antwerpen, Universiteitsplein 1, B-2610 Wilrijk, Belgium
and IIHE, ULB–VUB, Pleinlaan 2, B-1050 Brussels, Belgium
and Service de Physique des Particules Elémentaires, Faculté des Sciences, Université de l'Etat Mons,
Av. Maistriau 19, B-7000 Mons, Belgium
[y] Department of Physics, University of Liverpool, P.O. Box 147, Liverpool L69 3BX, UK
[z] Dipartimento di Fisica Sperimentale, Università di Torino and INFN, Via P. Giuria 1, I-10125 Turin, Italy
[α] Dipartimento di Fisica, Università di Bologna and INFN, Via Irnerio 46, I-40126 Bologna, Italy
[β] NIKHEF-H, Postbus 41882, NL-1009 DB Amsterdam, The Netherlands
[γ] Department of Radiation Sciences, University of Uppsala, P.O. Box 535, S-751 21 Uppsala, Sweden
[δ] Dipartimento di Fisica, Università di Genova and INFN, Via Dodecaneso 33, I-16146 Genoa, Italy
[ε] Department of High Energy Physics, University of Helsinki, Siltavuorenpenger 20 C, SF-00170 Helsinki 17, Finland
[ζ] Physics Department, University of Oslo, Blindern, N-1000 Oslo 3, Norway
[η] Dipartimento di Fisica, Università di Milano and INFN, Via Celoria 16, I-20133 Milan, Italy
[θ] Dipartimento di Fisica, Università di Padova and INFN, Via Marzolo 8, I-35131 Padua, Italy
[ι] Rutherford Appleton Laboratory, Chilton, Didcot OX11 0QX, UK
[κ] Ames Laboratory and Department of Physics, Iowa State University, Ames IA 50011, USA
[λ] Niels Bohr Institute, Blegdamsvej 17, DK-2100 Copenhagen Ø, Denmark
[μ] Institute for Nuclear Studies, and University of Warsaw, Ul. Hoża 69, PL-00681 Warsaw, Poland
[ξ] Physics Department, National Technical University, Zografou Campus, GR-15773 Athens, Greece
[π] High Energy Physics Laboratory, Institute of Nuclear Physics, Ul. Kawiory 26 a, PL-30055 Cracow 30, Poland

Received 9 May 1990

The pair production of the lightest scalar Higgs boson, h, and a pseudoscalar Higgs boson, A, was searched for in a data sample containing 10 000 hadronic Z^0 decays. The search involved both leptonic and purely hadronic decay channels of each Higgs boson. No signal was found, and limits on the Higgs boson masses, in the framework of the minimal supersymmetric extension of the standard model, ar reported up to 35 GeV/c^2 at 95% CL, for both $\tan\beta > 1$ and $\tan\beta < 1$, where $\tan\beta$ is the ratio of the vacuum expectation values of the two Higgs doublets.

1. Introduction

As often emphasized, LEP offers a unique opportunity to test experimentally the existence of the Higgs sector. The standard model predicts at least one neutral scalar of unknown mass but does not forbid the existence of extra Higgs isospin doublets or singlets which could give rise to physical charged or neutral Higgs bosons [1,2]. Direct searches for the standard model Higgs particle [3] and for charged scalars [4] have been recently performed by our collaboration.

Supersymmetry offers a good motivation to search

for such objects, since this model needs at least two neutral scalars h and H, one pseudoscalar A and a pair of charged scalars $H^{\pm}$. In the frame of what is usually referred to as the minimal supersymmetric extension of the standard model (MSSM) [2], couplings and even masses are highly constrained. The lightest particle is h with $m_h < m_Z$. All masses and couplings can be expressed in terms of m_h and of the angle β, $\tan\beta$ being the ratio of vacuum expectations generated in the two doublet model. In particular α, the mixing angle between the two neutral scalars, is determined and in the mass range under consideration, is approximately equal to $-\beta$. Conversely, once m_h and m_A are fixed, there exist two complementary determinations of β, β_1 and β_2 with $\tan\beta_1 = \cot\beta_2$.

The two Higgs bosons h and A can be produced in association, with the partial width in this model:

$$\Gamma(Z^0 \to hA) = \tfrac{1}{2}\lambda^3 \cos^2(\alpha-\beta)\, \Gamma_{\nu\bar{\nu}},$$

where λ is the phase space factor:

$$\lambda = [(1 - x_h^2 - x_A^2)^2 - 4x_h^2 x_A^2]^{1/2},$$

$$x_h = m_h/m_Z, \quad x_A = m_A/m_Z$$

and where

$$\cos^2(\alpha-\beta) = \frac{m_h^2(m_Z^2 - m_h^2)}{m_A^2(m_Z^2 + m_A^2 - 2m_h^2)},$$

with $\Gamma_{\nu\bar{\nu}}$ the partial width for the pair production of one neutrino species.

When $m_A \sim m_h$, one has $\cos^2(\alpha-\beta) \sim 1$ and the production rate is maximal. This situation occurs when $\tan\beta$ differs from 1. For instance, $\cos^2(\alpha-\beta) \sim 0.5$ corresponds to $\tan\beta \simeq 2.5$ (or $\tan\beta \simeq 0.4$), in which case one has $m_h \simeq 0.7 m_A$.

The Björken process $Z \to hZ^*$ also occurs in the model but is suppressed by a factor $\sin^2(\alpha-\beta)$ compared to the standard model prediction. If $\tan\beta$ turns out to be close to 1, this process has the most favorable yield and one recovers the standard picture.

For masses below the charm–anticharm threshold, the most interesting decay modes are those involving two charged particles in the final state. The predicted partial width into the $\mu^+\mu^-$ channel is well known but large uncertainties prevail on the $\pi^+\pi^-$ final state [5]. Therefore a phenomenological approach was used, looking at all possible exclusive channels below 2 GeV/c^2 and using the LUND prediction for the decay of higher mass gluon–gluon and $s\bar{s}$ states. Previous searches have already been performed in this mass range, in the decays of π, K, B and $\Upsilon(1S)$ particles [5]. Although no signal was observed, the derived limits are model dependent and cannot completely exclude the presence of a Higgs boson in this mass range. On the contrary, the present search is free, within the MSSM, from all the theoretical uncertainties concerning the Higgs boson production rate.

For masses above the charm–anticharm threshold, the scalar and pseudoscalar Higgs particles will decay preferentially into $\tau\bar{\tau}$, $c\bar{c}$ and $b\bar{b}$ with branching ratios given [1] in terms of the fermion masses and of the mixing angles α and β. One has:
for h

$$\mathrm{BR}(h \to \tau\bar{\tau} : b\bar{b}) = 1 : 2.1\,(\cot\alpha \cot\beta)^2 : 19\beta_b^3,$$

for A

$$\mathrm{BR}(A \to \tau\bar{\tau} : c\bar{c} : b\bar{b}) = 1 : 2.1\,(\cot\beta)^4 : 19\beta_b^3,$$

where β_b is the velocity of the b quark in the Higgs boson rest frame.

In case $\tan\beta > 1$, $c\bar{c}$ is suppressed and $\tau\bar{\tau}$ will dominate h and A decays below the $b\bar{b}$ threshold. Above this threshold, the $\tau\bar{\tau}$ branching fraction is about 6% for both Higgs bosons. In contrast, if $\tan\beta < 1$, hadronic modes are predominant in the whole mass range.

QCD corrections become very large only in a narrow mass region, very close to the $b\bar{b}$ threshold. Recently [6], the effect has been computed both for h and A with the conclusion that A is the most affected. If $\tan\beta \simeq 1$, the effect is confined in the mass range $9 < m_A < 11$ Gev/c^2.

From the previous discussion, there are two complementary approaches to search for neutral Higgs bosons. When $\tan\beta \simeq 1$, the standard process $Z \to hZ^*$ is optimum and results from our search for the standard model Higgs boson [3] can be directly applied. If $\tan\beta$ differs from 1, $Z \to hA$ becomes more appropriate if $m_h + m_A < m_Z$. In case $\tan\beta > 1$, as favoured by theory [1,2], tagging of heavy Higgs particles is possible through the $\tau\bar{\tau}$ final state. This is no more possible when $\tan\beta < 1$, a challenging case since the mode hA has to be searched for in purely hadronic

final states, containing charmed quark jets.

This paper combines several experimental techniques in an attempt to cover the various scenarios mentioned above. The analysis is based on data collected by the DELPHI detector, during the energy scan of the Z^0 performed at LEP at the end of 1989.

2. Detector

A detailed description of the DELPHI detector, of the trigger conditions and of the analysis chain can be found in ref. [7]. Here, only the specific properties relevant to the following analysis are summarized.

The charged particle tracks are measured in the 1.2 Tesla magnetic field by a set of three cylindrical tracking detectors: the inner detector (ID) covers radii 12 to 28 cm, the time projection chamber (TPC) from 30 to 122 cm, and the outer detector (OD) between 197 and 206 cm. The end-caps are covered by the forward chambers A and B, at polar angles 10° to 36° on each side. A layer of time-of-flight (TOF) counters is installed for triggering purposes around the cryostat containing the superconducting solenoid.

The present analysis relies primarily on charged particle tracks reconstructed using the TPC, complemented by the ID and OD detectors. This system reconstructs 98% of the charged particles down to polar angles of 30°. In some small azimuthal regions which correspond to the six boundaries of TPC sectors, this efficiency drops for energetic ($p>4$ GeV/c) particles. The momentum resolution varies from $\Delta p/p = 2\cdot 10^{-3}\times p$ (GeV/c) for tracks measured in the TPC only.

The electromagnetic energy is measured in the high density projection chamber (HPC) and by the forward electromagnetic calorimeters (FEMC) in the end caps. The HPC is a high granularity lead gas calorimeter covering polar angles 40° to 140°. For fast triggering, a layer of scintillation counters is installed after the first 5 radiation lengths of lead. The FEMC consists of 2×4500 lead glass blocks (granularity 1×1 degree), covering polar angles from 10° to 36° on each side.

The trigger is based on the ID and OD coincidences, on the HPC and TOF counters, and on the forward detectors. The track trigger is formed using opposite quadrants of the OD in coincidence with the ID trigger layer. The counter trigger uses half length quadrants of TOF counters sensitive to penetrating particles, and HPC counters sensitive to electromagnetic showers with an energy greater than 2 GeV, arranged in various sets of back-to-back and majority logics. The forward trigger is made from the same-side chambers A and B coincidences, combined with the FEMC signals from both sides in a majority logic. The efficiency of these various triggers is measured with the Z^0 data, by analysing the recorded trigger pattern, and is applied to the simulated data. The trigger efficiency in the barrel region thereafter is found to be over 99% for all hadronic Z^0 decays and four prong final states, and therefore does not play any critical role in the following analysis.

3. Data sample

Hadronic events were selected as follows:
- the number of charged particle tracks had to be at least five,
- the angle between the reconstructed thrust axis and the beam had to be greater than 37°, i.e. $|\cos\theta| < 0.8$,
- all the charged particle tracks had to form at least two clusters, as defined by the LUND cluster algorithm [8], used with default parameters. This cut is very efficient to eliminate beam gas events.

The charged particle tracks were considered if their momentum exceeded 100 MeV/c and if their extrapolated distance to the vertex, in the transverse plane and along the beam axis was less than respectively 4 cm and 5 cm.

The preceding cuts applied to the 1989 data sample collected around the Z^0 mass led to the selection of 9599 hadronic decays.

Low multiplicity events (two to four charged tracks) were selected in the same angular region and with the same track selection criteria.

4. h–A search for $\tan\beta > 1$

4.1. $\tau\bar{\tau}$ + hadrons final state

Events were searched for in which either the h or the A decayed through a $\tau\bar{\tau}$ pair. Such final states are characterized by the presence of two low multiplicity

jets, called slim jets hereafter, and one or two normal jets depending on the Higgs boson mass.

Jets were defined as charged particle clusters, reconstructed by the LUND jet algorithm [8], used with default parameters.

When each Higgs boson mass is below ~ 30 GeV/c^2, the two slim jets are to be found in the same hemisphere, opposite to the hadronic jets. The event is thus divided into two hemispheres according to the plane perpendicular to the thrust axis. Above this mass, the slim jets are still isolated from the hadronic jets but the hemispheric separation is lost.

The selection criteria were thus defined as below:

(i) Either two slim jets and one or two hadronic jets.

(ii) Or one slim jet and two hadronic jets.

For case (i), at least one of the slim jets must contain only one charged particle. Its energy has to be above 3 GeV. The other one can contain up to three charged particles, to allow for the three prong decay modes of the τ lepton and some level of contamination of a slim jet by a low momentum fragment of a hadronic jet. When a slim jet contains more than one particle, its mass is required to be below 2 GeV/c^2, and the two slim jets are required to be in the same hemisphere and their combined energy to exceed 90% of the hemisphere energy.

Case (ii) is relevant in two different domains:

(a) When one Higgs boson mass is sufficiently large so that one of the slim jets is buried in one hadronic jet. The analysis is quite similar to the one used in the charged Higgs search and described in detail in ref. [4]. Requiring the angle between the two hadronic jets to be below 90° removes the background from normal hadronic decays.

(b) When one Higgs boson mass is sufficiently low so that the two leptonic jets are merged into a single slim jet. In this case the slim jet is required to consist of two particles of energy higher than 1 GeV, of opposite charge and forming a jet with a mass above 2 GeV/c^2. Futhermore, the slim jet must contain all the energy of its hemisphere.

The efficiencies for these selection criteria were computed by a Monte Carlo program using a hA generator based on LUND Jetset 6.3 for subsequent hadronisation. Gluon radiation was generated when the Higgs decayed into a $q\bar{q}$ pair. Each Higgs could decay either into a $b\bar{b}$ pair or to a $\tau\bar{\tau}$, with the appropriate branching ratios for the h and the A. These efficiencies are displayed in table 1 for different masses of the Higgs bosons. The total efficiency is reasonably constant in the whole domain with a mean value of 33%.

The preceding cuts were then applied to the data sample. Fig. 1 refers to case (i) and shows the distribution of the sum of the hemisphere energy fractions carried by the two slim jets. The dashed area is the Monte Carlo prediction of a Higgs signal, which would give a prominent peak around 1. No candidate remains with an energy fraction above 90%. Fig. 2 refers to case (iib) and shows the mass distribution for events containing a jet made of a pair of oppositely charged particles, hemispherically isolated. Here also, the Higgs and the observed distribution differ significantly and no event passes the cuts with a jet mass above 2 GeV/c^2.

In summary, no candidate was found in any of the selected topologies. From a Monte Carlo study, the expected number of background events is 0.6 ± 0.3. Limits can therefore be set at the 95% confidence level in the m_h–m_A plane (fig. 3a).

For each point in the plane, the h–A partial width and the h and A branching ratios into $\tau\bar{\tau}$ are computed as given in the introduction. The efficiency is interpolated from the numbers displayed in table 1. The obtained 95% CL contour sets limits at the level of 35 GeV/c^2 except for large A masses and low h mass. However, this domain can be covered by looking at the reaction $Z^0 \to hZ^*$, where the limits obtained in the search [3] for the standard model Higgs can be used. This negative search leads to the exclusion contour plotted as dashed line in fig. 3a. The combined exclusion contour is such that Higgs bosons with masses up to 35 GeV/c^2 are thus excluded at a confidence level of 95%.

4.2. Four charged particles final state

This final state is relevant when both Higgs boson masses are below the $b\bar{b}$ threshold i.e. 10 GeV/c^2. A large part of this domain is already excluded by the $Z^0 \to hZ^*$ search (fig. 3a). In the remaining domain, the production rate is large and would yield around 500 Higgs boson pairs.

In this region, two prong decays from the $\tau\bar{\tau}$ channel become dominant below the charm threshold for

Table 1
Detection efficiency (in %) for various Higgs boson masses (in GeV/c^2).

m_h	m_A	Case			Total
		(i)	(iia)	(iib)	
5	20	28	6	1	35
20	20	23	4	3	30
12	30	25	3	6	33
20	30	29	5	2	37
35	35	21	0	8	29

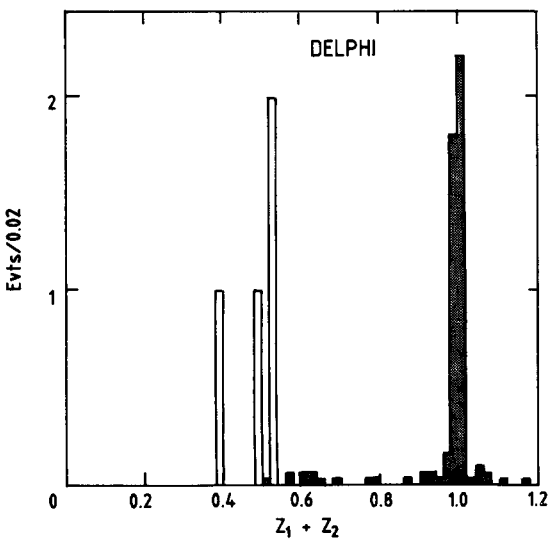

Fig. 1. z_1+z_2 distribution, where z_i is the energy carried by each slim jet divided by the total energy found in the hemisphere in which the slim jet was observed. One slim jet must contain only one charged particle track and the other two or three. The data are presented by the solid histogram, while the expected signal corresponding to h–A production, when both Higgs bosons have a 20 GeV/c^2 mass, is represented by the hatched area.

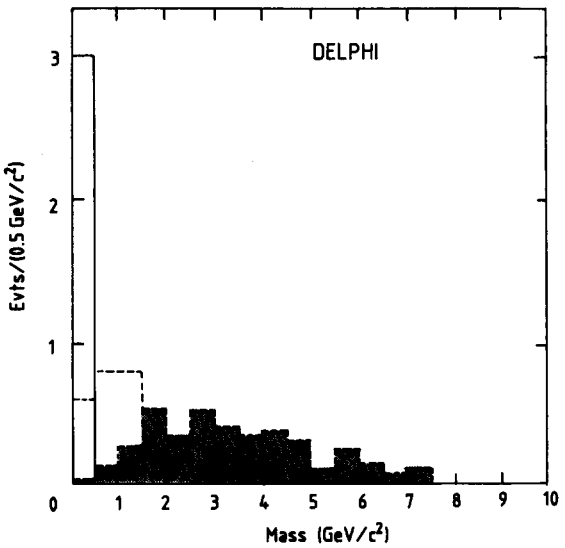

Fig. 2. Invariant mass of a pair of opposite charged particles recoiling against two hadronic jets. The data are represented by the full line, the expectation from udscb events by the dashed line. The hatched area corresponds to the signal that would be produced by a pair of 20 GeV/c^2 Higgs bosons.

tan $\beta < 1$ and up to the beauty threshold for tan $\beta > 1$. Since only low masses are involved, events containing four charged particles, with two tracks in each hemisphere were searched for. After requiring a zero total charge for the event, only one event is left. The angle between the beam and the thrust axis is found to be smaller than 40° and the ratio between the momenta of the two tracks found in the same hemisphere is found to be below 0.1. This event is therefore unlikely to be a Higgs candidate since the angular distribution of the Higgs events should be proportional to $\sin^2\theta$ and hence dominant in the barrel region, and the energy of the two tracks coming from a Higgs decay should be well balanced. The predicted branching fraction of a Higgs boson into a pair of charged particles is well known from 210 MeV/c^2 (the $\mu^+\mu^-$ threshold) to 300 MeV/c^2 (the $\pi^+\pi^-$ threshold) and, for tan $\beta > 1$, between 4 and 10 GeV/c^2, when the $\tau\bar{\tau}$ channel is dominant. Between 300 MeV/c^2 and 4 GeV/c^2, the gluon–gluon channel plays an important role [9], and especially until around 2 GeV/c^2. In this region between 300 MeV/c^2 and 2 GeV/c^2, the relative abundance of all the

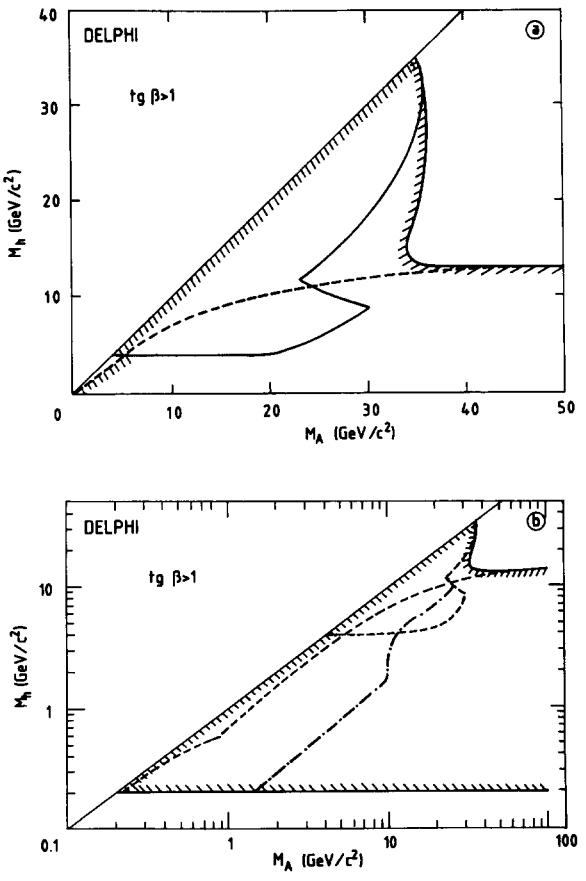

Fig. 3. Exclusion contours obtained for $\tan\beta > 1$. (a) The solid line corresponds to the region excluded by the $\tau\bar{\tau}$ analysis and the dashed line corresponds to the region excluded by the hZ* search. The hatched contour gives the combined exclusion limit. (b) Exclusion contour in the low mass region. The dashed curves are reproduced from (a). The dash–dotted curve corresponds to the four prong analysis. The hatched contour gives the combined exclusion limit.

allowed exclusive channels was computed using the isospin conservation rule which applies in the case of a strong decay mediated by two gluons. The pseudoscalar Higgs boson A decays are found to be dominated in this mass range by the $\mu^+\mu^-$ channel since the two or three pion decays are not allowed. In this region a conservative branching fraction of 45% into two prongs is used, in good agreement with other similar studies [10]. Above 2 GeV/c^2, the LUND 6.3 prediction was used for the gluon–gluon and the $s\bar{s}$ channels and yielded comparable two prong branching fractions in both channels decreasing from 45% at 2 GeV/c^2 to 15% at 4 GeV/c^2.

For Higgs boson mass below 500 MeV/c^2, the two decay particles are emitted very close to each other and are likely to be merged in a single track by the reconstruction program. Using the deposited ionisation in the TPC, it was checked that no single track in two prong events gave an ionization compatible with twice the deposition of a minimum ionizing particle.

The 95% CL contour deduced from the four prong analysis is reported in fig. 3b, together with the limits obtained with the low mass standard model Higgs search [3]. The excluded domain completely covers the Higgs boson mass range, from 210 MeV/c^2 to the beauty threshold.

5. h–A search for tan $\beta < 1$

In this domain, the two Higgs bosons dominantly decay into a $c\bar{c}$ pair. The final state looked for is thus formed by four charmed jets. Two approaches have been used to search for such events: the first one is based upon charm tagging, while the second relies on the four jet topology.

5.1. Charm tagging

The charm tagging method relies on the peculiar kinematic properties of the decay $D^{*+} \to \pi^+ D^0$. The low Q value of this decay forces the π^+ to be aligned with the D* line of flight and, therefore, the p_t distribution of this low momentum pion has a mean value of 30 MeV/c, instead of the universal 300 MeV/c, where p_t is the transverse momentum with respect to the jet axis. Furthermore, the pion momentum is an almost constant fraction (7%) of the D* momentum and is therefore around 4% of the jet momentum. This method was pioneered by the HRS group [11] at PEP and has been shown [12] to be applicable to multijet events produced at the Z^0.

The shaded histogram in fig. 4a shows the p_t^2 distribution obtained from a $Z^0 \to hA$ simulated sample, where both Higgs have a 20 GeV/c^2 mass and decay to $c\bar{c}$. Only events where four jets were reconstructed, using the LUND cluster algorithm [8], were retained. The transverse momentum was then com-

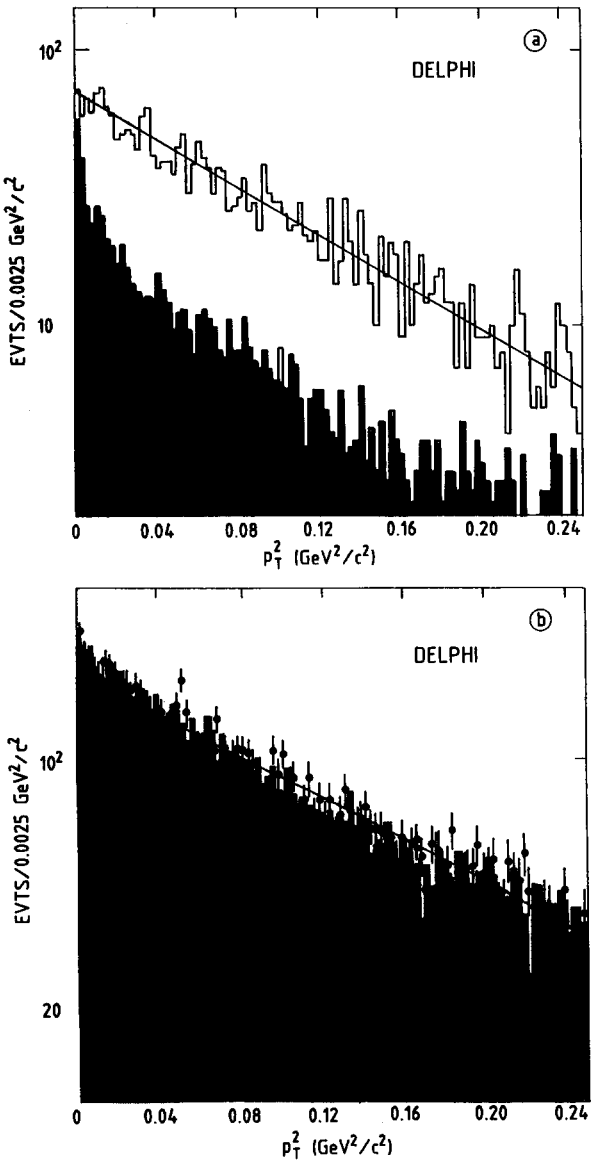

Fig. 4. p_t^2 distribution of charged particle tracks relative to their jet axis. (a) The dashed histogram is obtained by the simulation of a pair of 20 GeV/c^2 Higgs bosons decaying into $c\bar{c}$ pairs, using four jet events. The solid histogram is the corresponding distribution in our data sample. The solid line is the fit to this distribution obtained using two exponential functions of p_t^2. (b) Distribution obtained on two and three jet events. The points correspond to the real data, the light-shaded histogram to the udscb Monte Carlo prediction and the dark-shaded histogram to the $c\bar{c}$ contribution only. The solid line is the fit obtained using two exponential functions as in (a).

puted for each track with respect to the jet axis obtained using all the other tracks found in the same jet. In this way, the possible bias towards low p_t that could have been induced by including the track itself in the jet axis computation was removed. Only tracks with a momentum between 5% and 10% of the visible jet energy were considered. The resulting efficiency for h–A events using the charm tagging method is $(23 \pm 3)\%$. The solid histogram in fig. 4a shows the p_t^2 distribution obtained in the data sample. No signal was found and an upper limit of 30 D* candidates can be set at the 95% confidence level, using a fit to these data with two exponentials indicated by the solid line.

The efficiency of this method is almost mass independent and leads to the exclusion contour A in fig. 5. To gain complete confidence in this result, the same method was used to search for the normal charm–anticharm decays of the Z^0. A clear D* peak was obtained containing 102 ± 27 events is displayed on fig. 4b. Both the slope of the signal and its yield are in good agreement with standard model expectations (light-shaded histogram). The dark-shaded histogram represents the $c\bar{c}$ contribution with the characteristic peak due the D* meson. It is interesting to note that the D* tagging efficiency obtained by this

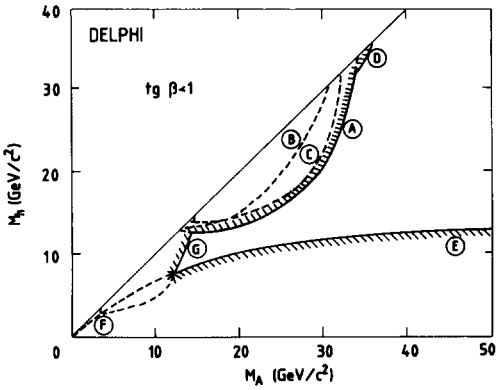

Fig. 5. Exclusion contours obtained for $\tan\beta < 1$. The labelled contours are obtained with the following analyses: Contour A: inclusive D* tagging. Contour B: four jet final state (using the method of ref. [4]. Contour C: four jet final state. Contour D: Thrust analysis. Contour E: hZ* production. Contour F: four prongs final state. Contour G: Tracks at large angle from the thrust axis. The hatched contour corresponds to the combined excluded region.

method is, as expected, five times larger than the one obtained by full exclusive reconstruction of the charmed meson, using the decay chain $D^{*+} \to \pi^+ + D^0 \to \pi^+ + K^- \pi^+$.

5.2. Four jet topology

The four jet method described in detail in our $H^\pm$ search [4] can be applied here when the two Higgs bosons have comparable masses. To start with, only mass differences between the two Higgs bosons up to 6 GeV/c^2 were considered, since the production cross section falls off rapidly when these two masses become very different from each other. This leads to the exclusion contour B in fig. 5.

In a second search, also based on hadronic four jet final states, the requirement of comparable masses for the two Higgs bosons was relaxed. The method relies on constructing the invariant masses of all pairs of jets in each four jet event, exploiting energy and momentum conservation constraints to improve the mass resolution for the jet pair masses. The associated production of the Higgs bosons was then searched for as a peak in the Dalitz plot of jet pair mass versus jet pair mass.

In the analysis, both charged particle tracks and calorimeter information from the HPC were used. The resulting subset of the data contains 4600 hadronic events.

For the clusters recorded in the electromagnetic calorimeter, the energy was required to be larger than 0.2 GeV.

In addition, the sphericity axis of the event was required to fulfill $|\cos\theta| < 0.6$. This cut enhances the signal to background ratio for the expected signal, as the angular distribution of the Higgs bosons is proportional to $\sin^2\theta$. A four jet reconstruction method was applied which maximises the four-thrust [13] (a generalized form of the standard thrust).

Given the four reconstructed jets, energy and momentum conservation constraints for the full event were then used to compute rescaling coefficients for the momenta of the jets. It was assumed that the directions of the jet axes were correctly measured. The coefficients determined in this way were generally of the order one, otherwise the event did not fit well the hypothesis of four jets, or these were nearly coplanar. A cut in the rescaling coefficients c_j, $0.5 < c_j < 2.5$, was applied.

Finally, the three pairs of jet–jet masses were calculated for each event, and for each pair, the smallest di-jet mass, M_s, was plotted versus the largest, M_ℓ.

The quality of the reconstruction of the jet–jet masses can be judged from fig. 6a, which shows the result of applying the four jet reconstruction and rescaling to simulated $Z^0 \to hA \to c\bar{c}c\bar{c}$ events, where

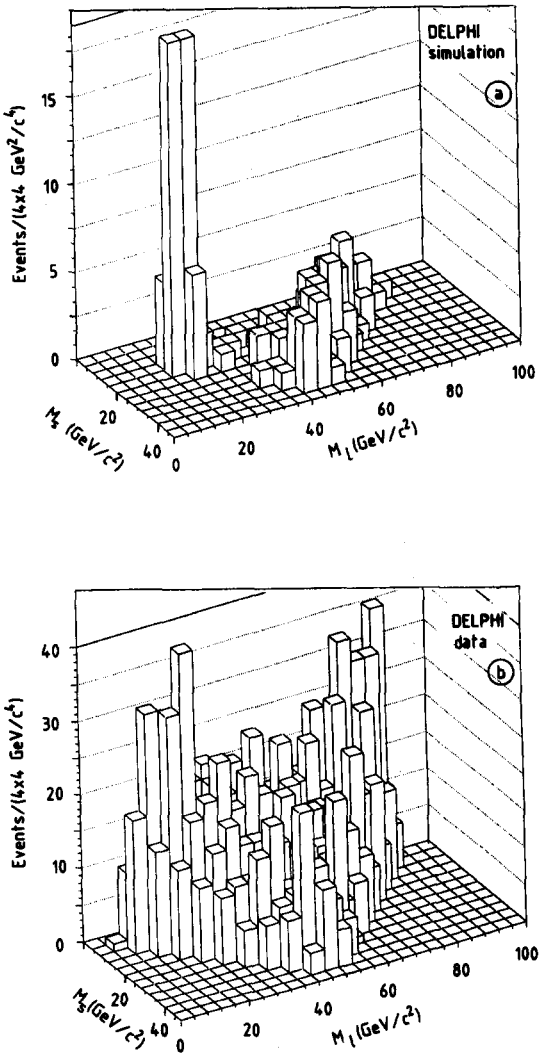

Fig. 6. Dalitz plot of the smallest M_s, and the largest M_ℓ invariant jet–jet masses for four jet final states. (a) From the simulation of the production of a pair of 20 GeV/c^2 Higgs bosons. (b) For the data.

$m_h = m_A = 20$ GeV/c^2. A clear peak is observed at average masses $M_s \approx 19$ GeV/c^2, $M_\ell \approx 20.5$ GeV/c^2, with a resolution of less than 2 GeV/c^2. The difference in the mean values of M_s and M_ℓ is due to the ordering of the masses. The wrong mass combinations are seen to contribute to a broad band of entries at large values of M_ℓ. The statistics in the plot has been chosen to correspond to the expected number of events in a sample of hadronic Z^0 decays of the present size.

The data (fig. 6b) clearly show no prominent peaks of the size of the simulated signal, apart from the structures at values of M_s around 10 GeV/c^2. These are due to artificially split two jet events and are well reproduced by a Monte Carlo simulation of standard $q\bar{q}$ events. The data sample itself is used to derive limits for the associated production of two Higgs bosons. The mass resolution and reconstruction efficiency for the hypothetical signal has been evaluated at $m_h = m_A$, with values ranging from 10 GeV/c^2 to 40 GeV/c^2. For $m_h \neq m_A$, the minimum of the detection efficiencies evaluated at the two mass values was conservatively used. Since the expected signal had a much narrower distribution than the observed variations in the density over the Dalitz plot, limits were derived for the maximum possible signal in the data at a nominal set of m_h, m_A values by subtracting a QCD background evaluated in a large region (20×20 GeV$^2/c^4$) around (m_h, m_A).

The resulting contour corresponding to m_h, m_A values that can be excluded at 95% CL is show as C in fig. 5.

When the Higgs boson mass increases, the jet reconstruction methods become less efficient. However, for a mass above 35 GeV/c^2, the events become so spherical that a thrust cut becomes powerful. The 95% CL limit can therefore be slightly extended (contour D) in the large mass domain, by requiring a thrust less than 0.75.

5.3. Low mass search

The exclusion limit obtained from the standard model Higgs search [3] applies also the case $\tan\beta < 1$ exactly in the same manner as in the case $\tan\beta > 1$ and is represented by the contour E in fig. 5. For the low mass region, the analysis reported in section 3.2

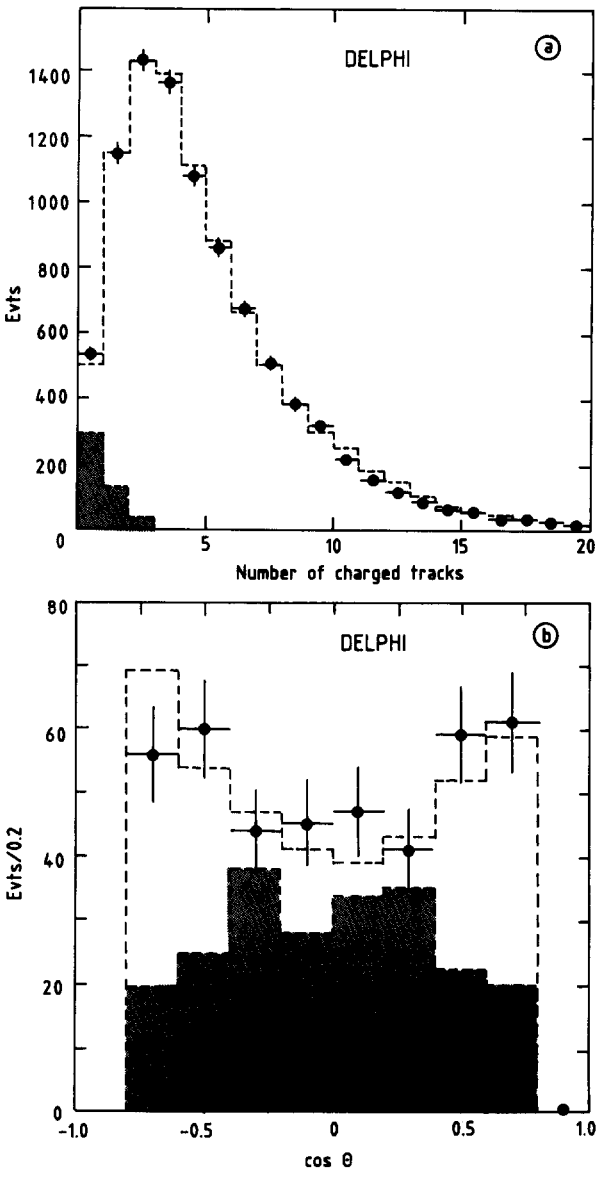

Fig. 7. (a) Distribution of the number of charged particles with momentum below 2 GeV/c observed at more than 40° from the thrust axis. The points represent the data, the dotted histogram the udscb prediction and the hatched area would correspond to the production of a pair of 10 GeV/c^2 Higgs bosons decaying into a a $c\bar{c}$ pair. (b) Angular distribution with respect to the beam axis of the thrust axis, for the two jet events containing no tracks emitted at large angle of the thrust axis. The points show the data, the dashed histogram the udscb prediction, and the shaded histogram the contribution of a pair of 10 GeV/c^2 Higgs bosons decaying into a $c\bar{c}$ pair.

is valid only below the charm threshold and corresponds to the contour F.

Above the charm threshold, a method based on the difference in the fragmentation process between a hA event and a $q\bar{q}$ event was used. In the former, no coloured string is stretched between the two Higgs bosons, whilst in the latter, such a string has been observed through its breaking, which leads to the production of low momenta particles at large angles with respect to the thrust axis. Therefore the multiplicity distribution of charged particles with momentum below 1 GeV/c, emitted at more than 40° from the thrust axis was studied (fig. 7a). A good agreement is observed between the data points and the udscb Monte Carlo prediction (dashed histogram), while Higgs production (shaded histogram) would lead to a strong enhancement in the first bin which is not observed. The Monte Carlo prediction based on the Lund 6.3 parton model describes the data correctly, giving support to the string fragmentation model on which it is based. The general characteristics such as multiplicity, total energy, thrust of the events with no particles emitted at large angle are also in good agreement with the udscb prediction. Fig. 7b shows the angular distribution of the thrust axis of these events. Background events from $q\bar{q}$ sources should follow a $1+\cos^2\theta$ distribution while events coming from Higgs production should follow a $\sin^2\theta$ dependence. Good agreement is observed between the data points and the udscb prediction (dashed histogram), while the contribution from a pair of 10 GeV/c^2 Higgs bosons represented by the shadowed area is not observed. From these results, the 95% CL exclusion contour G in fig. 5 was derived. These limits were checked to be quite insensitive to both the angular and momentum cuts used in this analysis. A 20% systematic error due to the uncertainty concerning the Higgs fragmentation process was taken into account.

6. Conclusion

Neutral Higgs boson pair production was searched in Z^0 decays using a large variety of possible final states and negative results are obtained. Limits are given in the framework of the minimal supersymmetric extension of the standard model in terms of the masses of the Higgs bosons h and A, for the two possible cases $\tan\beta > 1$ and $\tan\beta < 1$. They are summarized in fig. 8 where the 95% CL excluded region is shown in the plane (m_h–$\tan\beta$), using our best limits from the various analyses presented in this paper. This is the first time that such high mass limits are reported [14] in the case $\tan\beta < 1$. Higgs bosons are excluded from 210 MeV/c^2 up to 35 GeV/c^2 in a large domain of the parameters. Since these searches cover a wide variety of possible final states, ($\tau\bar{\tau}$, $c\bar{c}$, four jet events), the results are still constraining outside the MSSM models, although precise mass limits would have to be derived in each specific case.

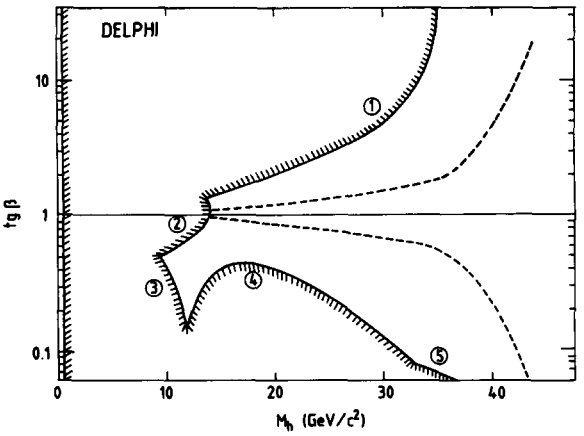

Fig. 8. Exclusion contours in the plane (m_h–$\tan\beta$). The hatched contour corresponds to the excluded region. In the MSSM model, the allowed parameters values are those to the left of the dashed line [1]. Contour 1: Combined limit obtained in section 3. Contour 2: hZ* production from ref. [3]. Contour 3: Contour G obtained in section 4.3. Contour 4: Contour A obtained in section 4.1. Contour 5: Contour D obtained in section 4.2.

Acknowledgement

We are greatly indebted to our technical staffs and collaborators and funding agencies for their support in building the DELPHI detector and to the members of the LEP Division for the speedy commissioning and superb performance of the LEP collider.

References

[1] P.J. Franzini et al., Z^0 Physics at LEP 1, Higgs search, CERN Report CERN 89-08, Vol. 2, p. 59.
[2] S. Dawson, J.F. Gunion, H.E. Haber and G.L. Kane, The physics of Higgs bosons: Higgs hunter's guide (Addison Wesley, Menlo Park, 1989).
[3] DELPHI Collab., P. Abreu et al., CERN/EP 90-44, to be published.
[4] DELPHI Collab., P. Abreu et al., Phys. Lett. B 241 (1990) 449.
[5] See the review in: Z^0 Physics at LEP, Higgs search, CERN Report CERN 89-08, Vol. 2, p. 72, and references therein.
[6] M. Drees et al., preprint CERN TH-5393 (1989).
[7] DELPHI Collab., P. Aarnio et al., Phys. Lett. B 231 (1989) 539; The Delphi Detector, to be published.
[8] T. Sjöstrand, Comput. Phys. Commun. 27 (1982) 243; 28 (1983) 229;
T. Sjöstrand and M. Bengtsson, Comput. Phys. Commun. 43 (1987) 367.
[9] M.B. Voloshin, Sov. J. Nucl. Phys. 44 (1986) 478.
[10] P. Janot, preprint LAL 89-45 (1989).
[11] P. Baringer et al., Phys. Lett. B 206 (1988) 551;
S. Abachi et al., Phys. Lett. B 205 (1988) 411.
[12] G. Wormser, preprint SLAC-PUB-4576 (1988).
[13] Sau Lan Wu, Z. Phys. C 9 (1981) 329.
[14] ALEPH Collab., D. Decamp et al., Phys. Lett. B 237 (1990) 291; B 241 (1990) 141.